

# SHOCK-PROTECTION OF NANO-GAP CAPACITIVE MEMS ACCELEROMETERS USING SLOPED ELECTRODE DESIGN

Yaesuk Jeong<sup>1,2</sup>, Michael Foster<sup>2</sup>, Junghun Chae<sup>2</sup>, Diego E. Serrano<sup>2</sup> and Farrokh Ayazi<sup>1,2</sup>

<sup>1</sup>Georgia Institute of Technology, Atlanta, GA, USA

<sup>2</sup>Qualtré Inc., Marlborough, MA, USA

## ABSTRACT

This paper presents a novel sloped electrode scheme to enable the implementation of shock stops in MEMS devices that use a sacrificial layer to define in-plane capacitive gaps. Since the thickness of the sacrificial layer grown or deposited on the sidewall of a microstructure is constant, by sloping the interdigitated fingers, one can get a larger travelling range for the proof-mass than the thickness of the sacrificial layer. This allows the realization of larger sensing gap than the shock stop without using additional photomasks or fabrication steps. Proposed scheme is incorporated into the accelerometer design with 270 nm gaps and number of different characterizations were done to verify the survivability of the sensor under high-g environment. Further characterization shows a scale factor of 55.3 mV/g, noise density level of 187.09  $\mu\text{g}/\sqrt{\text{Hz}}$  at 1 Hz for devices with a full-scale range of +/- 16g.

## INTRODUCTION

The increasing demand for high performance MEMS inertial sensors in emerging applications such as wearables, IoT, and personal navigation, has fueled the utilization of high aspect ratio (>100:1) sub-micron sensing gaps [1]. As the electromechanical transduction of capacitive MEMS device is heavily dependent on the electrode geometry, the sensor performance can be improved by scaling down the gap size, without relying on a large proof-mass. Therefore, fabrication processes that enable sub-micron lateral gaps in a relatively thick microstructure using sacrificial processes (e.g., HARPSS) are of great interest [2],[3], and have been successfully utilized to fabricate a variety of devices, such as gyroscopes [4], accelerometers [5], and resonators [6].

These devices are used in applications where the structures are subjected to extreme shock and random vibration. For example, a single free-fall from 1-meter height can create a sudden acceleration that is larger than 1,000 g (9,800 m/sec<sup>2</sup>) [7]. Under these circumstances, the displacement of the MEMS device could exceed its operating range such that the generated stress gets larger than the fracture strength of the structural material, causing a permanent damage to the microstructure. Under such conditions, if the proof-mass collides with the sense electrode, the impact could generate debris that can result in malfunctioning and electrical shorts [8]. Therefore, most of MEMS devices are equipped with shock stop to provide over-range protection [7][9]. Shock stop structures have smaller gap size than the sense electrode to limit the proof-mass movement and thus keep the generated stress within elastic region. Furthermore, as the shock stop is electrically

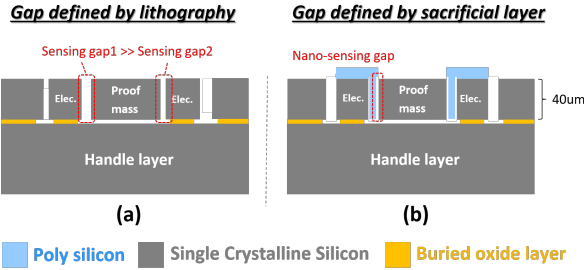


Figure 1. Comparison between fabrication processes using (a) lithography [10] and (b) sacrificial layer [5] to define gap size

tied to the proof-mass, an impact will not cause electrical problems in the readout circuits.

However, implementing a shock stop using a process, in which the gaps are defined by the sacrificial layers (e.g., SiO<sub>2</sub>) can be a challenging task, as its thickness is uniform across the entire wafer (Figure 1). To create sacrificial layers with different thicknesses, one may require to increase the number of photomasks and use additional fabrication steps, ultimately increasing the production cost.

In this paper, we present a novel sloped electrode design, which focuses on adjusting the geometry to implement multiple nano-gap sizes without additional fabrication processes. The proposed scheme was incorporated into an in-plane accelerometer as a proof of concept and number of different characterizations were conducted to validate its survivability and effectiveness under high-g environment.

## SLOPED ELECTRODE DESIGN

Figure 2 shows the schematic diagram of proposed sloped electrode, where interdigitated fingers are tilted so that its normal vector is at angle  $\theta_e$  with respect to the device motion. Assuming the device moves only along the Y- axis, the required traveling distance to make contact with the sense electrode (i.e., effective gap) can be derived using equation (1), where  $thk_{sac}$  is the sacrificial layer thickness.

$$d_{\text{effective}} = \frac{thk_{sac}}{\cos \theta_e} \quad (1)$$

Even if the sacrificial layer thickness  $thk_{sac}$  is constant over the entire device (single deposition), equation (1) shows that different effective gap sizes are still attainable by changing the angle  $\theta_e$  on the electrode. For the region that requires minimum gap (i.e., shock stop), the microstructure can be designed so that its normal vector is parallel with the device motion. On the other hand, for the sensing regions

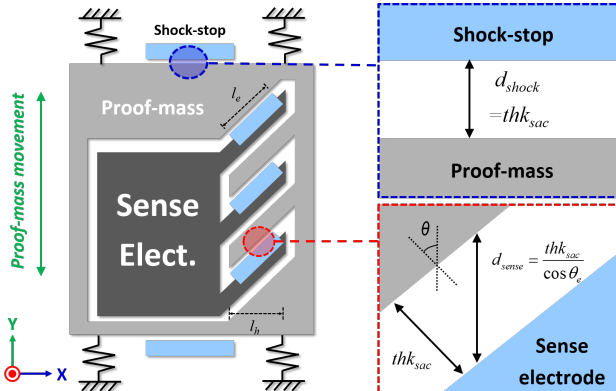


Figure 2: Schematic diagram of proposed sloped electrode, and zoomed-in views on shock stop and sensing electrode

where larger gap is needed, the angle  $\theta_e$  can be increased to widen the effective travelling distance of the proof-mass.

It should be noted that the capacitance change on the sloped electrode is the combination between parallel-plate ( $\theta_e = 0^\circ$ ) and comb-finger ( $\theta_e = 90^\circ$ ) sensing. Equation (2) shows the capacitive sensitivity of the sloped electrode accelerometer, where  $\epsilon_0$  indicates permittivity,  $H$  is device thickness,  $N_e$  is the number of electrodes,  $l_e$  is electrode length,  $d$  is gap size, and  $\omega_0$  is the resonance frequency. Since an increase in electrode angle  $\theta_e$  reduces the device sensitivity by a factor of  $\cos\theta_e$ , the electrode length needs to be extended so that such reduction can be compensated for.

$$\frac{\Delta C}{a} \approx \frac{2\epsilon_0 N_e H}{\omega_0^2 d} \cdot \left( \frac{l_e}{d} \cos \theta_e + \sin \theta_e \right) \quad (2)$$

## DESIGN IMPLEMENTATION

The proposed sloped electrode scheme was incorporated into an in-plane accelerometer as shown in Figure 3. The design was fabricated on a 40  $\mu\text{m}$  thick silicon-on-insulator (SOI) wafer using HARPSS process and subsequently wafer-bonded to create hermetic environment [4]-[5]. As the in-plane gap is defined by the 270 nm thick sacrificial layer, the effective gap on two sense electrodes ( $C_P$  and  $C_N$ ) with 45° angle becomes 381.84 nm (Figure 4). The number of sensing fingers is equally distributed on both sides of fixed electrode to provide cross-axis sensitivity rejection using differential capacitance. When the proof-mass moves towards the  $X$ -axis direction, the capacitance at one side of the sensing electrode increases, whereas the other side decreases. This results in zero net capacitance change under cross-axis acceleration. The shock stop is a “U-shaped” microstructure that is covered with poly-silicon layer, so that its normal vector on each plane is parallel with all three axes (Figure 5). Doing so makes the effective gap size into minimum ( $thk_{ox}$ ), providing over-range protection against extreme shock on all three directions ( $X$ -/ $Y$ -/ $Z$ - axis).

Since the device operates under wafer-level vacuum-packaged environment (1~10 Torr), it may experience instability issues such as long settling time or large overshoot due to smaller damping coefficient. A set of

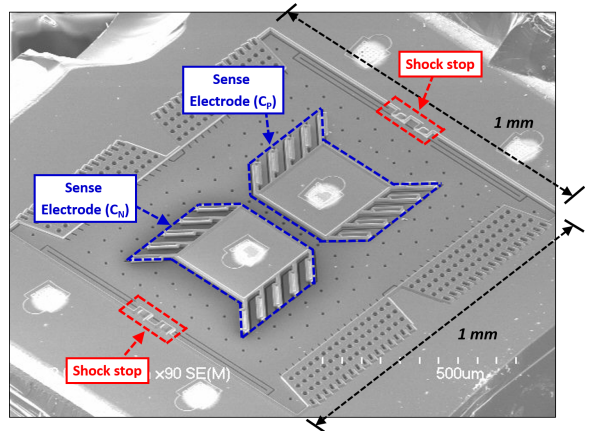


Figure 3: SEM picture of fabricated MEMS accelerometer incorporated with proposed sloped electrode design

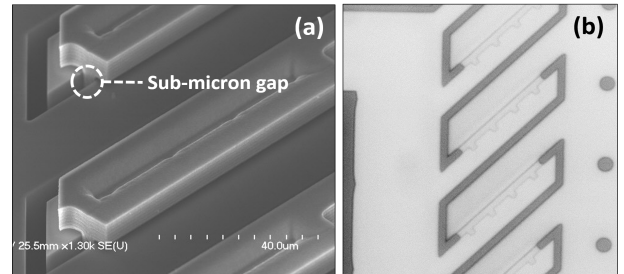


Figure 4. (a) SEM and (b) IR (Infra-red) microphotograph of sloped sensing electrode

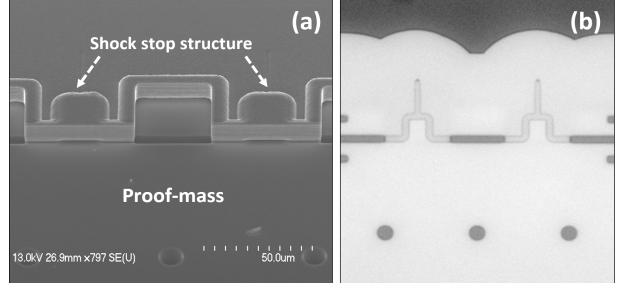


Figure 5. (a) SEM and (b) IR (Infra-red) microphotograph of shock-stop structure

additional sub-micron gap electrodes (known as damping electrodes) are placed at each side of proof-mass to increase the air-damping and ensure stable response [5]. Because the damping electrodes are electrically tied to the proof-mass potential, it acts as a control knob to adjust damping without affecting pull-in voltage. The damping electrode angle is reduced to 15° to improve the stability by taking squeezed-film-damping characteristic [11]. FEM analysis using ANSYS shows increased electromechanical coupling attained by narrow-gap, enables designing sensor with resonant frequency of 14.6 kHz, which corresponds to 1.16 nm displacement at 1-g acceleration. As a high resonant frequency structure is used, the proposed design can achieve full scale range of  $\pm 16$  g with small non-linearity of 0.36 %.

## MEASUREMENT

The effectiveness of the proposed sloped electrode scheme was verified by three types of measurements. First,

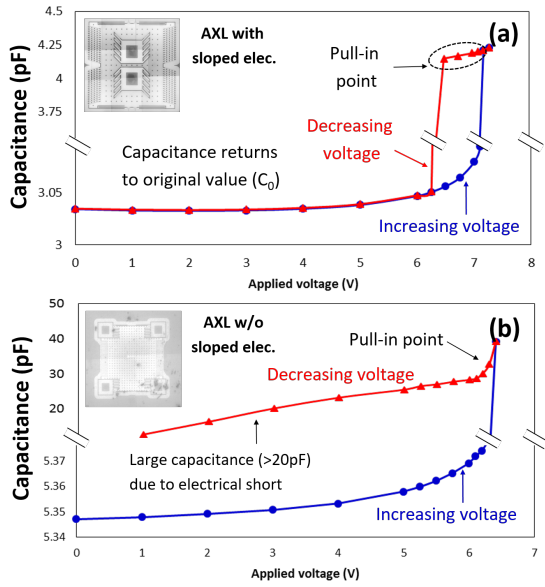


Figure 6. Pull-in behavior comparison between accelerometer (a) with and (b) without sloped electrode.

polarization voltage ( $V_p$ ) was swept on MEMS devices to mimic the extreme shock condition by creating an intentional pull-in, and measuring capacitance changes using Agilent 4284A LCR meter. For fair comparison, another accelerometer that does not use sloped electrode is also tested. This design [5] also uses parallel plate sensing with nano-gaps implemented using the same HARPSS process. However, all the capacitive gaps have the same effective gap distance with no shock stop.

Figure 6 compares the measured C-V response between two different designs. Once the pull-in occurs in the accelerometer with sloped electrode, the shock stop blocks the excessive movement on the proof-mass so that it does not make a direct contact with the sensing electrode. Because the device remains intact, the capacitance returns to its initial value ( $\sim 3$  pF) when the voltage is reduced after the pull-in (Figure 6(a)). On the contrary, for the accelerometer without sloped electrode, the proof-mass makes a direct contact with the sensing electrode, creating an electrical short so that the capacitance remains at much higher level ( $\sim 20$  pF) even after the voltage is reduced (Figure 6(b)). The measurement thus shows that the use of shock stop enabled by sloped-electrode prevents the collision between microstructure under extreme shock.

Additionally, the devices were attached to a metallic mass ( $m=0.2$  kg) and dropped from 1.8 m height to apply high-g acceleration. Peak acceleration generated during free-fall impact is expressed in equation (3), where  $COR$  is the coefficient of restitution,  $\Delta t$  the contact time during impact,  $g$  the earth gravity and  $H_d$  the free-fall height [7].

$$a_{peak} = \frac{1}{0.636} \cdot \frac{(COR+1) \cdot \sqrt{2gH_d}}{\Delta t} \quad (3)$$

Considering the impact time is between 0.2 to 1.2 ms [7], peak acceleration can be as large as 800 g ( $COR=0$ ,  $\Delta t$

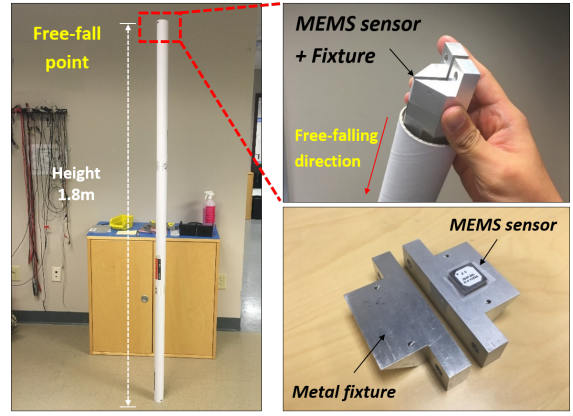


Figure 7. Photograph of free-fall measurement setup

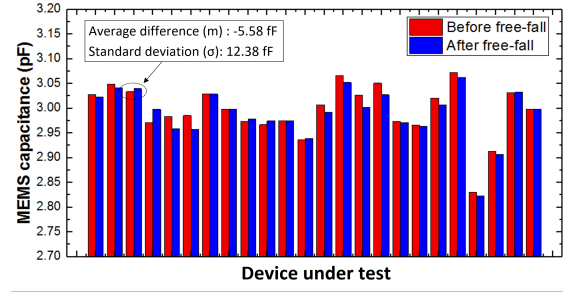


Figure 8. Comparison of measured static capacitances of MEMS accelerometer (a) before and (b) after the free-fall

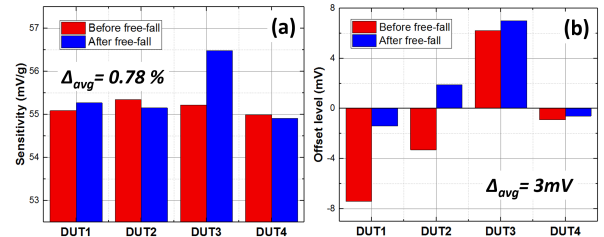


Figure 9. Comparison of measured (a) sensitivity and (b) offset level of MEMS+ASIC before and after the free-fall

$=1.2$  ms) to 9,500 g ( $COR=1$ ,  $\Delta t=0.2$  ms). The FEM analysis shows that under such high acceleration, the device displacement is large enough to make direct contact with the shock stop. The static capacitances ( $C_P$  and  $C_N$ ) of 12 devices are measured before and after the free-fall and compared on Figure 8, showing average difference ( $m$ ) of -5.58 fF, and the standard deviation ( $\sigma$ ) of 12.38 fF. Minor differences between data are caused by measurement error, such as different probe height. It should be noted that none of the device showed electrical short after the free-fall.

Finally, the accelerometer was wire-bonded to a switched capacitor ASIC and underwent high-g acceleration test to validate its effect on the sensor performance. Both sensitivity and offset levels of 4 different devices are measured before and after dropping from a same 1.8 m free-fall setup. Comparison plot on Figure 9 shows all the tested devices are still functional and experiences average variations of 0.78 % on sensitivity and 3 mV on offset level, which are mostly caused by the measurement errors. Considering minor changes on the output after the free-fall,

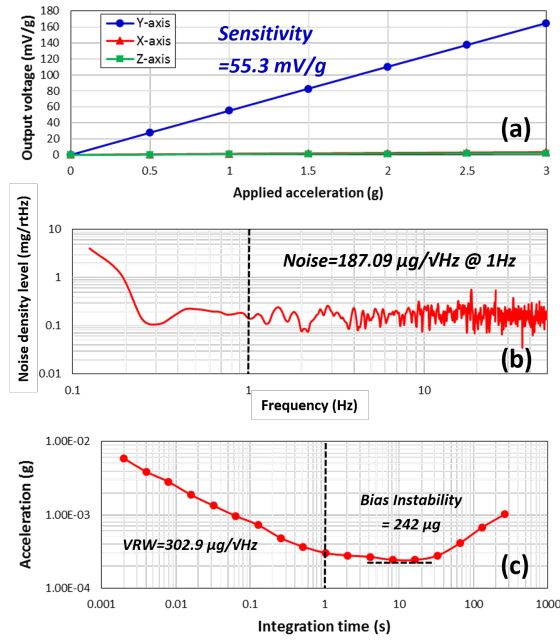


Figure 10. Measured (a) sensitivity, (b) noise density, and (C) ADEV plot of MEMS accelerometer



Figure 11. Step response of MEMS accelerometers under sudden acceleration ( $t=15$  ms)

it is concluded that high-g shock does not affect the accelerometer operation.

The overall performance of MEMS accelerometer are shown in Figure 10. The measured scale factor is 55.3 mV/g with cross-axis sensitivity of 2.13 % and 1.43 % on X- and Z- axis. Given that the simulated cross-axis sensitivity is less than 0.01%, alignment errors between the device and the evaluation board must be creating residual output signal. It should be noted that even though sloped electrode configuration is used, the cross-axis performance is not deteriorated thanks to using differential configuration. Figure 10(b) plots the noise density level, showing 187.97  $\mu\text{g}/\sqrt{\text{Hz}}$  at 1 Hz. The ADEV plot on Figure 10(c) shows bias instability of 242  $\mu\text{g}$ , and VRW (Velocity Random Walk) of 302.92  $\mu\text{g}/\sqrt{\text{Hz}}$ . The step response of the proposed accelerometer is shown in Figure 11. Because the shaker table setup has its own ringing behavior when applying sudden acceleration, the step response of a commercially available device (ADXL335) was also compared. Although proposed design operates under low-pressure level (1~10 Torr), it does not show instability and its step function responds similarly to ADXL335.

## CONCLUSIONS

A new sloped electrode configuration is presented in this paper, aiming at creation of multiple gap sizes using fabrication processes that utilize fixed sacrificial layer to define its high aspect ratio sub-micron gap. Such a scheme enables implementation of shock stops, which require smaller gaps than that of sense electrodes, without using any additional fabrication steps or photomasks. Further characterization on proposed scheme shows its effectiveness under high-g ( $>1,000$  g) environment.

## ACKNOWLEDGEMENTS

This work was supported in part by the DARPA Microsystems Technology Office, Single-Chip Timing and Inertial Measurement Unit (TIMU) program through SSC pacific contract #N66001-11-C-4176. Author would like to thank Qualtré and Anosh Daruwalla for their assistance.

## REFERENCES

- [1] F. Ayazi et al., "Multi-DOF inertial MEMS: From gaming to dead reckoning", *Transducers 2011*, pp. 2805-2808, 2011
- [2] F. Ayazi et al., "High aspect-ratio combined poly and single-crystal silicon (HARPSS) MEMS technology", *IEEE JMEMS*, vol. 9, pp. 288-294, 2000
- [3] J. Chae et al., "A monolithic three-axis micro-g micromachined silicon capacitive accelerometer" *IEEE JMEMS*, vol. 14, pp. 235-242, 2005
- [4] W. K. Sung et al., "A mode-matched 0.9 MHz single proof-mass dual-axis gyroscope", *Tranducers 2011*, pp. 2821-2824, 2011
- [5] Y. Jeong et al., "Wafer-level vacuum-packaged tri-axial accelerometer with nano airgaps" *MEMS 2013*, pp. 32-36, 2013
- [6] S. Pourkamali et al., "Vertical capacitive SiBARS" *MEMS 2005*, pp. 211-214, 2005
- [7] S. W. Yoon et al., "Shock-Protection Improvement Using Integrated Novel Shock Protection Technologies", *IEEE JMEMS*, vol. 20, pp. 1016-1031, 2001
- [8] D. M. Tanner et al., "MEMS reliability in shock environments", *IEEE Int. Rel. Phys. Symp.*, pp. 129-138, 2000
- [9] J. T. Suminto et al., "A wide frequency range, rugged silicon micro accelerometer with overrange stops", *MEMS 1996*, pp.180-185, 1996
- [10] B. V. Amini et al., "A high resolution, stictionless, CMOS compatible SOI accelerometer with a low noise, low power, 0.25  $\mu\text{m}$  CMOS interface", *MEMS 2001*, pp. 572-575, 2004
- [11] T. Veijola, et al., "Model for gas film damping in a silicon accelerometer", *Transducers 1997*, pp. 1097-1100, 1997

## CONTACT

Yaesuk Jeong: ys.jeong@gatech.edu